Available online at www.sciencedirect.com
SCIENCE DIRECT
Journal of Photochemistry and Photobiology A: Chemistry 180 (2006) 262–270
Journal of Photochemistry and Photobiology A:Chemistry
www.elsevier.com/locate/jphotochem

Model simulation of coherent laser control of the ultrafast spin-flip dynamics of matrix-isolated Cl_2

A.B. Alekseyev [a], M.V. Korolkov [b,c,*], O. Kühn [b], J. Manz [b], M. Schröder [b]

[a] *Theoretische Chemie, Bergische Universität Wuppertal, Gaussstr. 20, D-42097 Wuppertal, Germany*
[b] *Institut für Chemie und Biochemie, Freie Universität Berlin, Takustr. 3, 14195 Berlin, Germany*
[c] *B.I. Stepanov Institute of Physics, National Academy of Sciences of Belarus, Skaryna Avenue 70, 220602 Minsk, Republic of Belarus*

Available online 11 April 2006

Abstract

Starting from a diatomics-in-molecules Hamiltonian description of the valence states of Cl_2 embedded in an argon matrix, classical trajectory simulations are utilized to establish a one-dimensional model for the photodissociation dynamics in three selected singlet and triplet states which is valid during approximately 150 fs after Franck–Condon excitations, i.e. before the Cl atoms approach the neighbouring Ar atoms. Using this one-dimensional model which describes the dynamics of the Cl–Cl bond length in the frozen argon lattice we carry out quantum dynamics simulations of the laser pulse control of the electronic spin with femtosecond time resolution and sub-Ångstrom spatial localization by means of simultaneous excitation of wave packets on the singlet and triplet potential curves starting from a vibrational superposition state in the electronic ground state. It is shown that the latter can be prepared by a pump–dump pulse sequence.

Keywords: Coherent spin control; Matrix-isolated dihalogens; Spin–orbit coupling; Ultrashort laser pulses

1. Introduction

During the last years a variety of theoretical concepts of laser control of molecular processes have been turned into powerful practical methods. One of the very successful approaches is the method of coherent control, which has been pioneered by Brumer and Shapiro [1,2]. Specifically, they suggested to utilize quantum mechanical coherence related to interfering pathways between the initial and degenerate target states in order to control, e.g. the branching ratio in photoinduced unimolecular reactions. Another important development is due to Tannor, Rice and coworkers [3,4]. In their scheme two sequential pump- and dump- (or more generally pump- and control-) visible (VIS) or ultraviolet (UV) laser pulses are employed in order to initiate a reaction in an electronically excited state and to drive it to a specific target product in a different electronic state, depending on the time delay between the laser pulses. Today, the field of laser control is advanced, in particular in the experimental realization of feedback-driven optimal control [5,6] of systems ranging from gas- and condensed phase polyatomics [7] to biological complexes [8]. The apparent experimental success provides new challenges to theory not only to answer principal questions of controllability [9] but also to unravel the details underlying the dynamics which is triggered by an optimal laser control pulse, see e.g. [10], and to extend the available concepts into new domains of applications. Condensed phase systems are particularly demanding due to the disturbances of quantum mechanical coherences introduced by the interaction of the control target with its surroundings [7,11–13]. However, it has been shown recently, that this interaction itself can be controlled by means of phase-locked ultrafast laser pulses [14]. Moreover, this interaction may also work for the good, e.g. modifying the topology of the potential energy surfaces (PES) in a way as to support the desired reactions and processes [15,16]. In a recent study [17] of ClF embedded in a solid state argon matrix along the ⟨1 1 1⟩ direction, we have shown that the PES which are responsible for the dynamics of the Cl and F fragments after photoexcitation to the $^1\Pi$- and $^3\Pi$-states and subsequent bond stretching are modified from the dissociative topology in the gas phase to a quasi-bound, "cage" topology in the solid, see also Refs. [15,16]. Their near-degeneracy close to the cage walls or near the cage exits causes a rapid spin-flip in accord

* Corresponding author. Tel.: +49 3083854568; fax: +49 3083854792
E-mail address: korolkov@chemie.fu-berlin.de (M.V. Korolkov).

1010-6030/$ – see front matter © 2006 Elsevier B.V. All rights reserved.
doi:10.1016/j.jphotochem.2006.02.025

with experimental results of Schwentner and coworkers [18]. In fact this process occurs on a time scale of about 100 fs, i.e. before substantial energy is transferred into the matrix. This suggested that a simple one-dimensional model should be adequate for describing ultrafast laser-induced molecular spin-flip in matrices.

Motivated by the joint experimental and theoretical results of Ref. [17], and taking into account the importance of the spin–orbit coupling (SOC) between the $^1\Pi$- and $^3\Pi$-states, which is reflected already in violation of the spin selection rule for the $^1\Sigma$ to $^3\Pi$ optical transition, we have suggested a new scheme for coherent control of the spin state of a matrix isolated diatomic at a given time and bond length [15]. There, an infrared (IR) pulse prepares the diatomic molecule in a coherent superposition of two vibrational states in the electronic ground state. A subsequent ultrashort VIS pulse promotes the system simultaneously into the $^1\Pi$- and $^3\Pi$-states by resonant Franck–Condon transitions from the two vibrational states. This launches two coherent wave packets which propagate towards collision with matrix atoms (specified below), and which can interfere already on their way to the outer turning point. It has been shown that this interference can lead to a rapid change of the ratio between singlet and triplet state populations. The actual time dependence of this ratio can be controlled by the parameters of the exciting laser pulses. For instance, an important laser parameter is the delay time between the IR and VIS pulses, implying some analogy with the approach of Tannor et al. [3] (see also Refs. [19,20]), but instead of two VIS or UV laser pulses using IR + VIS ones in a different interference scheme. This spin control scheme can also be viewed as an extension of the original Brumer–Shapiro approach [1] to the case of time-dependent wave packets representing different near-degenerate molecular spin states which interact by SOC.

In this contribution we extend our previous study [15] of coherent spin control of matrix-isolated diatomics. To this end we will focus on Cl_2 that occupies a symmetric double-substitutional site in the argon matrix. On one hand, this system supports the reduced dimensionality as compared to the asymmetric ClF that resides in a mono-substitutional site. Moreover, we shall show that Cl_2 offers additional flexibility for control of the spatial location of the spin target state, compared to the previous investigation of ClF in Ar [15]. But on the other hand, the homonuclear Cl_2 poses an additional challenge because unlike ClF, its initial vibrational superposition state cannot effectively be prepared by means of an IR pulse. For this purpose one can, however, employ Raman type transitions [35], or design excitation schemes as shown in the present paper (see also: M. V. Korolkov, J. Manz, in preparation). Our investigation will start with classical dynamics simulations of the Cl_2 photodissociation dynamics in order to estimate the time domain where the diatomic's motion is effectively decoupled from the Ar matrix. This allows validating the model of reduced dimensionality that will be used in the subsequent quantum simulations of coherent spin control presented in Section 3. In Section 4, we give additional information on the possible preparation of the vibrational wave packet in the electronic ground state. The paper is summarized in Section 5.

2. Reduced dimensionality model

Diatomic molecules and in particular dihalogens embedded in low-temperature rare gas matrices continue to serve as model systems for condensed phase dynamics [11–18,21]. For the description of photoinduced processes which involve the coupled electronic and nuclear dynamics, the diatomics-in-molecules (DIM) approach has been shown to provide a reasonable compromise between accuracy and feasibility [22–25].

In the following we will focus on the case of Cl_2 in an argon matrix (for a DIM treatment of Cl_2 in xenon see Ref. [22]). The DIM Hamiltonian reads:

$$H = H_{\mathrm{mol}}^{\mathrm{Cl_2}} + \sum_{\mathrm{Cl},k} V_{\mathrm{Cl},k}(|R_{\mathrm{Cl}} - R_k|, \theta_{\mathrm{Cl},k}) + \sum_k T_k^{\mathrm{Ar}} + \sum_{k,l} V_{\mathrm{Ar}}(|R_k - R_l|) \quad (1)$$

Here, $H_{\mathrm{mol}}^{\mathrm{Cl_2}}$ is the Hamiltonian for the isolated diatomic which is described by the valence bond basis set consisting of 36 states. Nominally there are 9 singlet states and 27 triplet states which are mixed by spin–orbit interaction. For the latter we assume the Λ–S-level coupling scheme where we use a constant SOC such that the atomic Cl spin–orbit splitting of 0.109 eV [26] is reproduced. For the pure singlet and triplet adiabatic PES we use the results obtained earlier in the ab initio calculations of the free Cl_2 molecule [27,28]. In these studies the core electrons of chlorine atoms ($1s^2 2s^2 2p^6$) have been described by the relativistic effective core potential (RECP), so that only the $3s^2 3p^5$ outer electrons have to be treated explicitly via basis functions. To obtain the PES and corresponding wave functions at the Λ–S level of treatment a conventional multireference single- and double-excitation configuration interaction (MRD-CI) method with a configuration selection at an energy threshold of $T = 0.25\,\mu E_{\mathrm{h}}$ and energy extrapolation to $T = 0$ has been employed. The CI calculations have been carried out in the basis of molecular orbitals obtained in the self-consistent field calculation of the $^1\Sigma_{\mathrm{g}}^+(\sigma_{\mathrm{g}}^2 \pi_{\mathrm{u}}^4 \pi_{\mathrm{g}}^4)$ ground state. The importance of higher-than double excitations in the CI treatment has been assessed by applying the generalized multireference analogue of the Davidson correction. One should note that at this stage of the calculations all relativistic effects other than spin–orbit interaction are taken into account by means of the spin-independent part of the RECP (AREP). More technical details of the Cl_2 calculations can be found elsewhere [27].

The second term in Eq. (1) accounts for the isotropic and anisotropic interaction between the Cl and Ar atoms by means of pair potentials [29] (it depends on the distance between the nuclei as well as on the angle $\theta_{\mathrm{Cl},k}$ enclosed by the position vector of the electronic $2p_z$-orbital directed along the Cl–Cl bond at the Cl atom and the vector connecting the Cl with the k-th Ar atom). The actual interaction parameters have been taken from molecular beam scattering [30]. The third and last terms in Eq. (1) give the kinetic energy of the Ar atoms and the argon–argon interaction, respectively; the pair potentials are taken from Aziz and Slaman [31]. Having at hand the DIM Hamiltonian, the fully adiabatic PES for the nuclear motion in

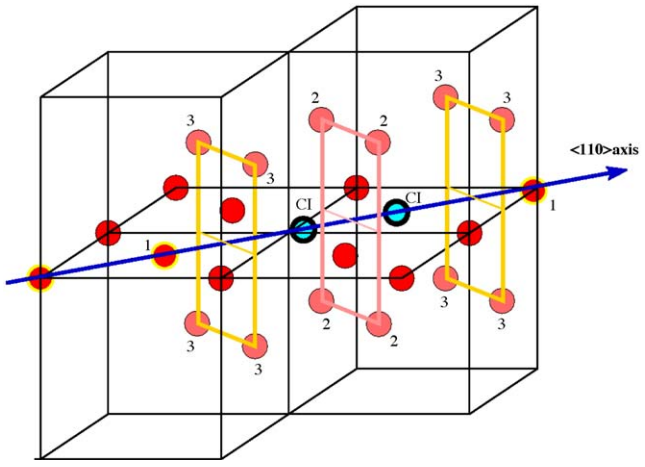

Fig. 1. Equilibrium geometry of Cl_2 on double substitutional site directed along the ⟨1 1 0⟩ direction in a face-centred cubic argon lattice. Important argon atoms of the immediate surrounding include the collision (1), the belt (2), and the window (3) atoms. The planes spanned by the belt and window atoms are shown as grey rectangles.

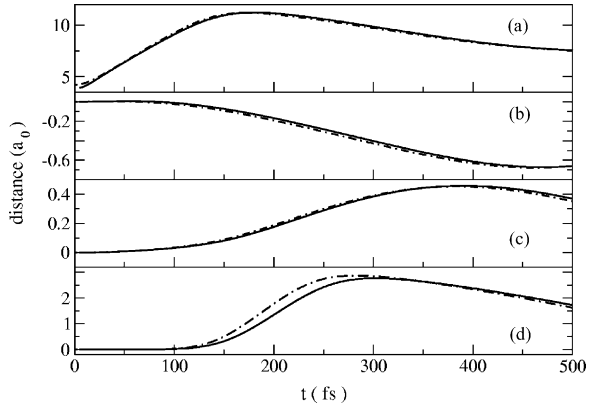

Fig. 2. Classical dynamics of interatomic distances after vertical Franck–Condon excitation from the potential minimum of Cl_2 in the ground state to the $^3\Pi$-state ($R_{Cl–Cl} = 3.98a_0$, dash-dotted lines) and to the $^1\Pi$-state from a displaced ground state geometry ($R_{Cl–Cl} = 4.2a_0$, solid lines): (a) Cl–Cl, (b) belt Ar atoms, (c) window Ar atom, (d) collision Ar atoms, cf. Fig. 1 (note the different scales). The matrix atom distances are defined by the deviation from the equilibrium position perpendicular (b and c) to and along (d) the Cl_2 axis.

the different electronic states can be obtained by diagonalization for any given position of the nuclei. By "fully adiabatic" we will characterize those states where the SOC is taken into account, i.e. there are only kinetic couplings between the different states (see, e.g. Ref. [25]). This representation is well suited for the propagation of classical trajectories with "on-the-fly" potentials. However, for the subsequent wave packet propagation we employ the equivalent but more convenient diabatic picture where the pure singlet ($^1\Sigma$, $^1\Pi$) and triplet ($^3\Pi$) potentials are coupled exclusively by SOC. This representation also facilitates a more intuitive characterization of the dynamics.

For the classical simulations a box containing besides the Cl_2 molecule 1272 argon atoms has been used with periodic boundary conditions [32]. Fig. 1 shows the equilibrium geometry which has been obtained by simulated annealing. The substitution site for the Cl_2 oriented along the ⟨1 1 0⟩ direction can be characterized by three different groups of Ar atoms, that is collision (1), belt (2), and window (3) atoms. For excitation energies above the gas phase dissociation limit the collision atoms can be expected to be the most important interaction partners. Now let us focus on the full-dimensional classical dynamics. We start with classical trajectories on the $^3\Pi$-state PES assuming a vertical excitation from the minimum of the ground state PES. The time-dependence of the Cl–Cl bond length and of the displacement from equilibrium for important Ar atoms (cf. Fig. 1) is shown in Fig. 2 (dashed-dotted lines). The dynamics of the Cl–Cl bond appears to be free up to about $11a_0$ at ca. 150 fs (cf. the linear time dependence in Fig. 2a). Afterwards one notices an appreciable motion of the lattice atoms and here primarily of the collision atoms. The interaction with the other atoms is much weaker in this initial time interval such that the belt atoms tend to move slightly into the site emptied by the Cl_2 while the windows open. For a more detailed study of the coupled Cl_2-matrix dynamics, see Ref. [33].

The dynamics upon excitation from a displaced geometry in the ground state ($R_{Cl–Cl} = 4.2a_0$) mimicking a vertical excitation from a vibrationally excited state to the $^1\Pi$-state (see Fig. 3) is also shown in Fig. 2 (solid lines). Apparently, the dynamics of the collision between the Cl atoms and the collision atoms resembles that of the $^3\Pi$-state case. This similarity of the dynamics on the $^3\Pi$- and $^1\Pi$-state PES also holds for the other types (belt, window) of argon neighbours.

Inspecting Fig. 2 we notice that prior to the first collision with the solvent cage the stretching of the Cl–Cl bond is almost decoupled from that of the Ar lattice. In other words, during the first ca. 150 fs after Franck–Condon like photoexcitation a one-dimensional description of the dynamics is justified, where only the Cl–Cl bond changes in the frozen Ar lattice. This is in accord with previous classical and quantum studies of F_2 in argon [13,25]. It also lends further support for the model used for ClF in argon [15–17]. In the following we shall employ a simple model of three coupled diabatic PES including the frozen argon atoms as shown in Fig. 3. This allows us to focus on important effects of the coherent spin control [15]. This model should serve as a reference for more sophisticated treatments

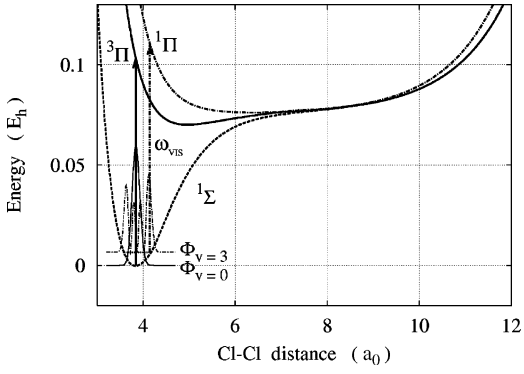

Fig. 3. Potential energy curves of the three relevant states ($^1\Sigma$, $^3\Pi$, $^1\Pi$) within the reduced one-dimensional model of the Cl_2 bond stretching. Also shown are the densities of two vibrational wave functions, which contribute to the initial state in Eq. (2). The VIS laser pulse excitation conditions are shown with arrows.

including couplings to additional electronic states and additional degrees of freedom.

The one-dimensional PES in Fig. 3 already allows anticipating some qualitative aspects of the collision dynamics. Promoting a classical particle (or a corresponding wave packet) from the ground state minimum ($R_{\mathrm{Cl–Cl}} = 3.98a_0$) to the $^3\Pi$- or $^1\Pi$-state by means of a vertical Franck–Condon type transition, the particle will find itself on a steeper potential curve in the $^1\Pi$-state as compared to the $^3\Pi$-state. At those vertical excitation energies the particle will move until the bond length is stretched to the outer turning point at ca. $11a_0$ in the $^1\Pi$-state or even larger distances for the $^3\Pi$-state. Of course, the initial acceleration is larger for the $^1\Pi$-state, i.e. the particle would hit the Ar collision atoms earlier. Coherent spin control requires, however, that the wave functions in the $^1\Pi$- and $^3\Pi$-states interfere in spin and phase space at the same time. For this purpose in the control scheme to be investigated in Section 3 a wave packet is launched on the $^1\Pi$-state but starting from a vibrationally excited level in the $^1\Sigma$ electronic ground state. Thus, a vertical transition in the sense of the classical trajectories would imply to start from a configuration where the Cl–Cl bond is slightly stretched ($R_{\mathrm{Cl–Cl}} = 4.2a_0$). In terms of the one-dimensional potential in Fig. 3 this leads to an initial configuration on the $^1\Pi$-state for which the gradient of the potential is even slightly less than that of the $^3\Pi$-state $R_{\mathrm{Cl–Cl}} = 3.98a_0$. Thus, if two trajectories would be started at the same time at $R_{\mathrm{Cl–Cl}} = 3.98a_0$ on the $^3\Pi$- and at $R_{\mathrm{Cl–Cl}} = 4.2a_0$ on the $^1\Pi$-states, they would "meet" when hitting the collision atoms around $11a_0$. The corresponding two quantum wave packets moving on the $^3\Pi$- and $^1\Pi$-states, however, will disperse such that one can anticipate that they interfere already during their approach of the potential wall due to the collision atoms.

The similarity of the marginal motions of the Ar atoms, which are induced by photoexcitation of Cl_2 to the $^1\Pi$- and $^3\Pi$-states, as documented in Fig. 2, suggests that any feedback from those Ar motions to the molecular wave packets representing Cl_2 should be comparable for the $^1\Pi$- and the $^3\Pi$-state.

3. Coherent spin control

Having established a one-dimensional model for the dynamics of the Cl_2 bond length which is valid during the first ~150 fs after Franck–Condon excitation to the $^3\Pi$- and $^1\Pi$-states, we will apply now a coherent control scheme similar to Ref. [15]. However, it will become clear shortly that the topology of the PES for Cl_2 in Ar offers the possibility to control the spin state in a time and spatial window within considerably larger domains as compared to ClF in Ar [15].

Fig. 3 shows the potential energy curves for the relevant states within the one-dimensional model introduced in the previous section. As compared to the case of ClF oriented along the ⟨1 1 1⟩ direction in Ar [15] the dissociating fragments do not hit the first window at a bond length of about $5.5a_0$, but the different geometry allows for passing through the respective first window (labelled (3) in Fig. 1) up to a bond extension of about $11a_0$ before they hit the collision atoms (labelled (1) in Fig. 1). Thus, the interference phenomena to be discussed below may take place within much larger domains of bond distances. Note the ClF oriented along the ⟨1 1 0⟩ direction will show a similar plateau-type PES as the one shown for Cl_2 in Fig. 3 [34].

The coherent control mechanism involves two steps: first, the laser pulse preparation of a coherent superposition state between two vibrational levels in the electronic ground state, specifically the vibrational ground state ($v = 0$) and the third excited state ($v = 3$), i.e.:

$$|\Psi_1(t=0)\rangle = c_0|\Phi_{v=0}\rangle + c_3|\Phi_{v=3}\rangle \tag{2}$$

In the following we will label the population of the vibrationally excited state as $r = |c_3|^2$, thus, the ground state population is $|c_0|^2 = 1 - r$. The phase difference of the complex coefficients in Eq. (2) is denoted as φ. The relevant vibrational densities for the case of Cl_2 are shown in Fig. 3. The parameter r can be determined from the condition of equal yields in the target excited electronic states. In the present case, a rather small fraction r in the excited state will be sufficient, typically $r \leq 0.01$. These coherent initial states may be prepared by means of Raman type transitions [35], see also the example in Section 4, or as a result of a single pulse nonlinear excitation (see also: M.V. Korolkov, J. Manz, in preparation). We postpone the discussion of the preparation to Section 4, use Eq. (2) as the initial state, and focus on the second step in the control scheme that is coherent excitation of the $^1\Pi$- and $^3\Pi$-states, see Fig. 3. For this purpose, we design a single VIS laser pulse of the form:

$$E(t) = E_0 \sin^2\left(\frac{\pi t}{\tau}\right)\cos(\omega_{\mathrm{VIS}} t), \quad \text{for } 0 \leq t \leq \tau \tag{3}$$

with amplitude E_0, duration τ (FWHM = 0.364τ), and carrier frequency ω_{VIS}. In addition we have assumed that the laser field is polarized along the direction of the transition dipole moment which is perpendicular to the molecular axis. The frequency is chosen such as to provide a simultaneous Franck–Condon transition between the vibrational ground state and the $^3\Pi$-state, $|\Phi_{v=0}, {}^1\Sigma\rangle \rightarrow |\Psi_3, {}^3\Pi\rangle$, as well as a corresponding vertical transition between the third excited vibrational state and the electronic $^1\Pi$-state, $|\Phi_{v=3}, {}^1\Sigma\rangle \rightarrow |\Psi_2, {}^1\Pi\rangle$, cf. Fig. 3.

The related wave packet dynamics is obtained by solving the coupled Schrödinger equation for the model which has been derived in Section 2:

$$i\hbar\frac{\partial}{\partial t}\begin{pmatrix}|\Psi_1\rangle\\ |\Psi_2\rangle\\ |\Psi_3\rangle\end{pmatrix} = \begin{pmatrix}T+V_1 & 0 & -\mu_{13}E(t)\\ 0 & T+V_2 & V_{\mathrm{SOC}}\\ -\mu_{31}E(t) & V_{\mathrm{SOC}} & T+V_3\end{pmatrix}\begin{pmatrix}|\Psi_1\rangle\\ |\Psi_2\rangle\\ |\Psi_3\rangle\end{pmatrix} \tag{4}$$

Here, we have labelled the ground-, $^3\Pi$-, and $^1\Pi$-state diabatic potential curves by V_1, V_2, and V_3, respectively. The SOC between $^3\Pi$- and $^1\Pi$-state is denoted by V_{SOC} and according to the selection rules for the pure diabatic spin states, there is only a nonvanishing transition dipole matrix element between the $^1\Sigma$ and the $^1\Pi$-state, $\mu_{13} = \mu_{13}(R_{\mathrm{Cl–Cl}})$ [28]. Finally, T is

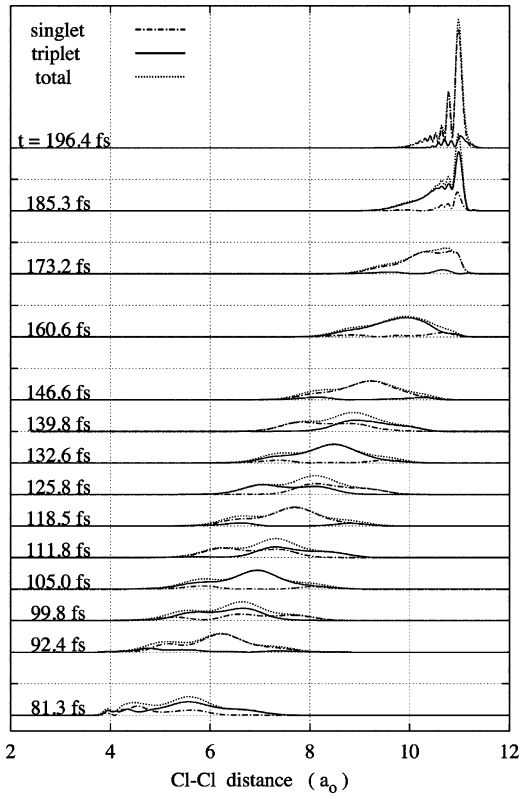

Fig. 4. Wave packet dynamics of the Cl_2 bond after excitation from a prepared vibrational superposition state (Eq. (2) with $r = 0.01$ and $\varphi = 0$) to the $^1\Pi$- and $^3\Pi$-states. The separate contributions from the $^3\Pi$- and $^1\Pi$-states as well as the total probability distribution are shown. The laser pulse parameters (cf. Eq. (3)) are $E_0 = 50$ MV/cm, $\tau = 100$ fs, and $\hbar\omega_{VIS} = 0.103 E_h$, ($\triangleq 22606\,cm^{-1}$). The propagation has been performed on a grid of 1024 points ranging from 2 to $16a_0$. The SOC constant between the diabatic singlet and triplet states corresponds to $588\,cm^{-1}$.

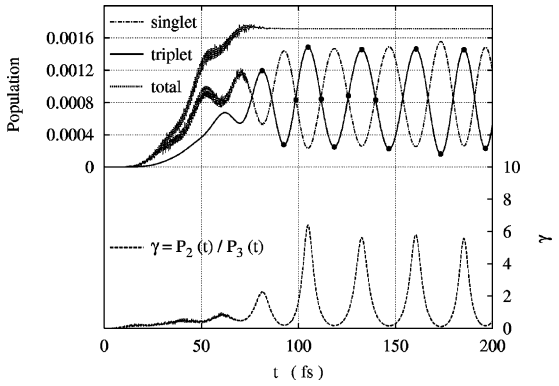

Fig. 5. Upper part: populations of the diabatic $^3\Pi$- (solid line) and $^1\Pi$- (dash-dotted line) state as well as the total electronic excited state population (dotted line) for the excitation conditions of Fig. 4. Lower part: related ratio between $^1\Pi$- and $^3\Pi$-state populations. The solid circles in the upper part correspond to the snapshots shown in Figs. 4 and 6.

the kinetic energy operator involving the reduced mass of the relative Cl_2 motion.

Fig. 4 shows snapshots of the dynamics, represented by the densities $|\Psi_i(R_{Cl\text{–}Cl}, t)|^2$ ($i = 2, 3$) and also the total densities in the excited states, as it takes place upon VIS excitation from the prepared state, Eq. (2), with $r = 0.01$, $\varphi = 0$ and $\tau = 100$ fs. Let us first consider the total densities for the two excited state potentials. As can be seen the wave packets propagate with changing shapes up to the outer turning point around $11a_0$ in about 200 fs. In view of our classical simulations in Section 2, this basically confirms our expectations. Also, at the outer turning point one observes the typical nodal structure reflecting the interference between the already reflected "front" and the still nonreflected "tail" of the wave packet which represent the turn from bond stretching to compression close to the outer turning points of the potentials, respectively.

The possibility of coherent spin control becomes apparent when inspecting the wave packets on the individual diabatic states also shown in Fig. 4 (compare solid and dashed-dotted lines). The total wave packet can be composed either of an almost pure singlet (e.g. at 92.4, 118.5, 146.6 fs) or an almost pure triplet (e.g. at 105.0, 132.6, 160.6 fs) contribution or with almost equal weights (e.g. at 81.3, 99.8, 118.5 fs). In other words, the population ratio:

$$\gamma(t) = \frac{P_2(t)}{P_3(t)} \tag{5}$$

is alternating with time. This is a consequence of the VIS excitation from the superposition state, Eq. (2), and of the design of a resonant VIS pulse which allows for a simultaneous excitation of two wave packets, $\Psi_2(t)$ and $\Psi_3(t)$, which overlap in position and momentum, that is, phase space (see below) as they approach the outer turning points of the cage potentials V_2 and V_3. The resulting interference is then mediated by SOC, leading to the observed change of the apparent spin character of the evolving quantum state.

Quantitative details of the change between singlet and triplet character of the wave function can be discussed by looking at the populations of the $^3\Pi$-($P_2(t)$) and $^1\Pi$-($P_3(t)$) states as plotted in Fig. 5. As anticipated from Fig. 4 these populations change quasi periodically with time. The approximate period of the associated spin flip is ~23 fs, in accord with the inverse energy gap of the two vibrational states which contribute to the initial state, $h/(E_{v=3} - E_{v=0}) = 23$ fs. This confirms the coherent nature of the interfering wave functions in the excited singlet and triplet states, originating from their simultaneous laser excitation from the initial state (2). For comparison, excitation from pure vibrational eigenstates $|\Phi_{v=0}\rangle$ or $|\Phi_{v=3}\rangle$ would result in much slower spin flips (ca. 300 fs), mediated by pure SOC, with much longer periods associated with the large amplitude vibrations in the potential energy curves of the electronic excited states. Similar effects have been discovered for ClF in Ar (see Fig. 3 of Ref. [15]). It is illuminating to compare these effects of molecules isolated in rare gas matrices with somewhat analogous ones for molecules in the gas phase, e.g., K_2 (cf. Ref. [36], see also [45]). There the oscillation period connected with the wave packet propagation is about 500 fs, much shorter than the oscillation period induced by SOC, ca. 3 ps.

Using the population ratio, Eq. (5), the purity of the spin state at a given time becomes even more apparent; see the lower part of Fig. 5. From the comparison of Figs. 4 and 5 it is obvious that, for instance, within a time window of about 20 fs around 105 fs

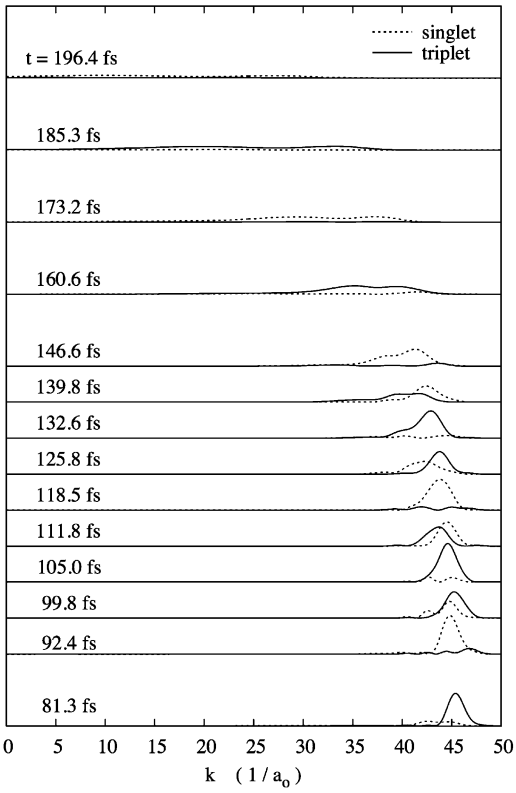

Fig. 6. Momentum space wave packet dynamics corresponding to the coordinate space representation of Fig. 4.

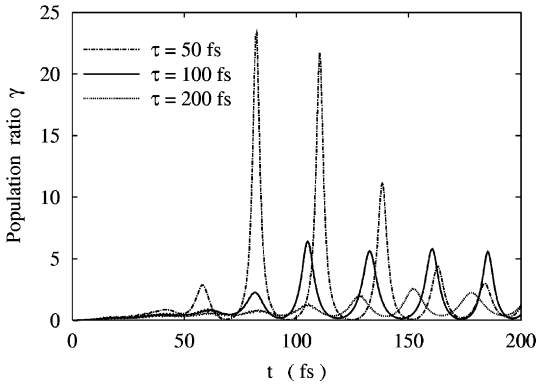

Fig. 7. Dependence of the population ratio, Eq. (5), on the duration τ of the VIS pulse for the conditions of Fig. 4.

the wave packet is an almost pure triplet and it is located in a narrow spatial window around $7a_0$. This quasi-localization in time and space should allow for observing this quantum state, e.g., by a probe pulse which induces a selective triplet-to-triplet transition with subsequent laser-induced fluorescence [17,18]. The rather low excitation efficiency of 0.0016 (see Fig. 5) could be enhanced, in the nonlinear excitation regime, to approximately $r = 0.01$ by means of more intense laser pulses. But even 0.0016 efficiency is sufficient for observing the laser-induced fluorescence from the ionic triplet state which are excited by means of pump-probe spectroscopy.

The notion of overlapping phase space distributions for the present spin control is supported by the wave packet dynamics in momentum space shown in Fig. 6. Accordingly, during the time window from ca. 80 to 150 fs the evolving wave packets do not only overlap in coordinate space but they overlap also in momentum space. Moreover, close to the outer turning point the wave packets are dispersed in momentum space from 0 to about $45a_0^{-1}$. The focussing of both singlet and triplet wave packets, of course, can be traced to the special preparation conditions, see Fig. 3, mimicking the classical trajectory simulations of Fig. 2.

In a next step, we would like to investigate the dependence of the coherent control scenario on the duration τ of the VIS laser pulse. After all the robustness of the large variations of the population ratio observed in Fig. 5 with respect to the laser parameters is an important point when it comes to a practical realization. In Fig. 7 we have plotted the population ratio, Eq. (5), as a function of the parameter τ. Apparently, shortening the pulse from the previously used l00 to 50 fs increases $\gamma(t)$ dramatically, in particular at short times. This is explained easily since a shorter pulse will launch more compact wave packets to the excited states such that the subsequent spatial overlap between the $^3\Pi$- and the $^1\Pi$-state is improved. However, wave packet dispersion in the anharmonic potential curves will wash out this effect and consequently, after about 160 fs the obtained population ratios for 50 and 100 fs pulse are comparable. On the other hand, for a longer pulse ($\tau = 200$ fs in Fig. 7) constructive interference yielding spatial localization is more difficult to achieve due to the dispersion of the wave packets.

Fig. 7 also reveals a dependence of the frequencies of the spin-flip oscillations on the pulse duration. This is not unexpected since the present system is not as simple as a three level model for which one would have only a single period of 23 fs corresponding to the energy difference between the initial vibrational wave functions, $h/(E_{v=3} - E_{v=0})$. Instead, the present use of a rather short VIS pulse implies a corresponding broad spectrum of many vibronic states in the coupled singlet and triplet potential curves, and the energy distribution and corresponding interferences of the evolving wave packet are rather sensitive to the pulse spectrum.

We anticipate that for longer propagation times ($t \gg 150$ fs) the effect of the initial preparation on the population ratio would be washed out due to the wave packet dispersion and energy dissipation from the excited molecule to the matrix environment. Accordingly, the present type of spin control cannot be achieved with nanosecond or CW lasers (as used in Ref. [1]), but it relies on ultrashort (below ~200 fs) laser pulses. We cannot, however, investigate the transition from ultrashort laser pulses to CW excitation, because the time domain $t > 150$ fs goes beyond the limit of our model. In passing we note that Bandrauk et al. have investigated the limit of continuous wave coherent control of Cl_2 in the gas phase [37].

Another important control parameter of the present scheme is the relative phase φ of the coefficients in Eq. (2). Fig. 8 shows the resulting population ratio γ depending on φ. Apparently, the preparation of specific phase shifts allows additional flexibility in control of the time and spatial windows during which the system is, e.g. in an almost pure triplet state. The possibility to control the relative phase, φ, and its relation to

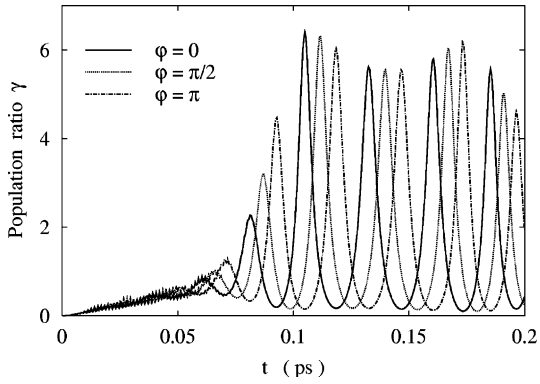

Fig. 8. Dependence of the population ratio, Eq. (5), on the relative phase between the components of the initial vibrational superposition state, Eq. (2), for the VIS pulse of Fig. 4.

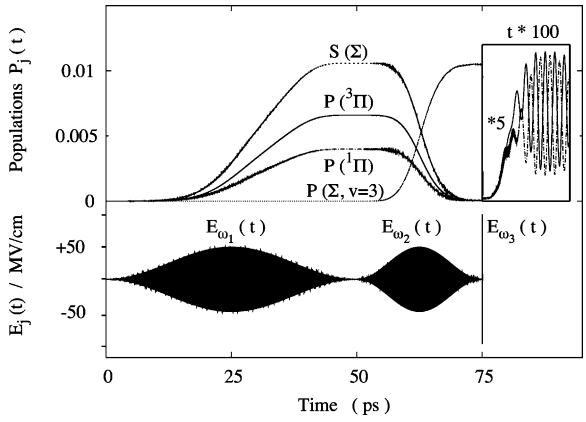

Fig. 9. Two-pulse scheme for the preparation of the initial $v = 3$ state in the electronic ground state. The inset shows the population dynamics triggered by the VIS control pulse (compare Fig. 5). The pulse parameter are $E_{0,1} = E_{0,2} = 5.1$ MV/cm, $E_{0,3} = 103$ MV/cm, $\hbar\omega_1 = 0.0756 E_h$, $\hbar\omega_2 = 0.069 E_h$, $\hbar\omega_3 = 0.103 E_h$, $\tau_1 = 50$ ps, $\tau_2 = 25$ ps, $\tau_3 = 0.1$ ps. The pulse intensities are $I_1 = I_2 = 3.5 \times 10^{12}$ W/cm^2, $I_3 = 1.4 \times 10^{13}$ W/cm^2. $\Sigma = 1 - P(\Sigma)$

the delay between IR and VIS pulses has been discussed in Ref. [15].

4. Initial state preparation

In the following we will address the issue of preparing the initial state, Eq. (2), which is a superposition of the vibrational ground and third excited state in the electronic ground state. Since Cl_2 has no dipole moment the direct IR excitation as proposed for ClF in Ref. [15] is not feasible. Instead one has to devise a scheme which involves the intermediate excitation of an electronically excited state. One possibility would be the pump–dump scheme of Tannor et al. [3] which has been realized, e.g., for preparing a narrow distribution of vibrational levels in the ground state of K_2 via a stimulated Raman scattering [35] (see also the simulations in Ref. [38]). A related approach, that is, the stirring of vibrational wave packet motion by "carving" a hole into the ground state wave packet has been discussed in Refs. [39,40]. An alternative strategy discussed in the literature employs partially overlapping nanosecond pulses for selective state population via a stimulated Raman process by adiabatic passage (STIRAP) [41].

The scheme which we present in the following is similar to the pump–dump like Raman experiment discussed in Ref. [35] with the difference being that we aim at exciting not a distribution of vibrational states but a single vibrational state. Apart from the different target state there are several important issues to consider: (i) in contrast to Ref. [35] we are dealing with a condensed phase situation where phase and energy relaxation might obscure the control efficiency, (ii) in order for our scheme to work we need only a rather small fraction of population in the state $|\Phi_{v=3}, {}^1\Sigma\rangle$.

In the following we will consider a specific Raman-type preparation of the initial state (2) via low-lying vibrational states in the triplet state, i.e. with the "Raman" laser pulse frequency tuned to the corresponding singlet-to-triplet transitions which are mediated by weak SOC. This strategy is motivated as follows: the strength of the interaction with the matrix environment increases if the energy of the excited state wave packet comes closer to the gas phase dissociation limit. This is reflected in the rapid increase of the widths of the phonon side bands as well as of the zero-phonon lines in the ${}^3\Pi \leftarrow {}^1\Sigma$ excitation spectra [42]. For instance, for the state $|\Phi_{v=7}, {}^3\Pi\rangle$ the linewidth of the zero-phonon line is about 3 cm^{-1} which corresponds to an electronic coherence dephasing time of about 1.8 ps (M. Fushitani, M. Gühr, private communication). Nothing is known about the lower lying vibrational states. For the population relaxation times in this spectral region one can estimate time scales in the range 1–2 ps which increase up to about 130 ps for the $|\Phi_{v=3}, {}^3\Pi\rangle - |\Phi_{v=4}, {}^3\Pi\rangle$ states [43].

This trend of increasing time scales for vibrational population relaxation when moving energetically deeper into the potential minimum of the Cl_2 triplet state is reasonable due to the reduced interaction with the Ar lattice [12]. The following model simulations which are again based on Eq. (4), make use of this fact by exciting rather low-lying vibrational states in the triplet state only.

The suggested pulse sequence is shown in Fig. 9 together with the relevant population dynamics. The first pulse, $E_1(t)$, prepares a spectrally very narrow wave packet close to the bottom of the ${}^3\Pi$-state potential. This wave packet is subsequently dumped by a second pulse, $E_2(t)$, to the $v = 3$ level of the electronic ground state. Notice that due to the SOC there is a transient population of the ${}^1\Pi$-state as well. However, the electronic excited states are depopulated at the end of the second pulse, i.e. by the time when the VIS control pulse, $E_3(t)$, is switched on. The pulse parameters (see figure caption) have been chosen such as to achieve the population of the target state which is required for the spin control scheme of Fig. 5. The respective electronic population dynamics after the control pulse is shown in the inset. The time scale required for this vibrational pre-excitation is far beyond the limits of the present model discussed in Section 2. But, notice that this limit was set by the first collision of the Cl atoms with the Ar lattice. For the suggested preparation scheme such a direct collision is not realized since the wave packet is confined to the bottom of the ${}^3\Pi$-state potential.

Therefore, the limiting factor would be extended from the (irrelevant) time of collision (ca. 150 fs) to the vibrational population relaxation time. For the scenario in Fig. 9 we assumed that it is longer than the pulse duration (FWHM) of about 27 ps. Clearly, more simulations including the effect of the matrix environment are needed to investigate appropriate pre-excitation mechanisms.

5. Conclusions and outlook

We have demonstrated coherently controlled wave packet dynamics in the $^1\Pi$ and $^3\Pi$ electronic states of Cl_2 in a solid argon matrix, starting from an initial vibrational superposition state consisting of the vibrational ground state plus a small fraction in the excited state ($v = 3$ and $r = 0.01$ in Eq. (2)). The investigation has been based on a diatomics-in-molecules Hamiltonian. Classical molecular dynamics simulations served to validate a one-dimensional description during the first ~150 fs after Franck–Condon excitation. The control target has been to prepare an almost pure spin state in a specific time and bond length window, beyond previous non-spin-selective schemes [17,44]. This has been achieved by means of a femtosecond VIS pulse which launches two coherent wave packets on the diabatic singlet and triplet curves such that they interfere in phase space corresponding to stretched Cl_2 bonds. These interferences in matrix environment are mediated by the rather large spin orbit coupling compared to the energy gap between the near-degenerate singlet and triplet states.

Thus, in the spirit of coherent control we have two interfering pathways leading from vibrational states in the electronic ground state to near-degenerate excited states, which overlap at a given time and with narrow spatial distribution in alternating spin states. These pathways are due to: (i) pre-excitation of a small population in a vibrationally excited state (Eq. (2)) followed by efficient VIS excitation to the singlet state and (ii) simultaneous weak VIS excitation from the vibrational ground state to the triplet Π-state, mediated by SOC. This results in an interference of the coherent wave packets with about equal initial populations of the singlet and triplet states. Subsequent interferences yield an ultrafast coherent oscillation of the spin character of the quantum state. The localized character of this state in phase space should facilitate an experimental observation, for instance, by appropriate placing the Franck–Condon window of a probe pulse for a transition into higher excited states such as the ionic manifold [17]. However, before this can be realized, further work is necessary to study pre-excitation mechanisms. A possibility which relies on a two-pulse pump–dump scheme has been discussed in Section 4. It may serve as a reference for the development of an efficient single-pulse nonlinear strategy for vibrational pre-excitation (see also: M.V. Korolkov, J. Manz, in preparation).

Acknowledgments

The authors gratefully acknowledge financial support by the Deutsche Forschungsgemeinschaft through the Sfb450 and in part by BRFFI (Φ 05MC-046) (M.V.K.) and the Fonds der Chemischen Industrie (J.M.). Further we would like to thank R.B. Gerber (Jerusalem) as well as N. Schwentner, M. Gühr, and M. Fushitani (Berlin) for stimulating discussions.

References

[1] P. Brumer, M. Shapiro, Chem. Phys. Lett. 126 (1986) 541.
[2] M. Shapiro, P. Brumer, Principles of the Quantum Control of Molecular Processes, Wiley, Hoboken, 2003.
[3] D.J. Tannor, R. Kosloff, S.A. Rice, J. Chem. Phys. 85 (1986) 5805.
[4] S. Rice, M. Zhao, Optimal Control of Molecular Dynamics, Wiley, New York, 2001.
[5] R.S. Judson, H. Rabitz, Phys. Rev. Lett. 68 (1992) 1500.
[6] I. Walmsley, H. Rabitz, Phys. Today 56 (2003) 43.
[7] T. Brixner, G. Gerber, ChemPhysChem 4 (2003) 418.
[8] J.L. Herek, W. Wohlleben, R.J. Cogdell, D. Zeidler, M. Motzkus, Nature 417 (2002) 533.
[9] H.A. Rabitz, M.M. Hsieh, C.M. Rosenthal, Science 303 (2004) 1998.
[10] C. Daniel, J. Full, L. González, C. Lupulescu, J. Manz, A. Merli, S. Vajda, L. Wöste, Science 299 (2003) 536.
[11] V.A. Apkarian, N. Schwentner, Chem. Rev. 99 (1999) 1481.
[12] V. May, O. Kühn, Charge and Energy Transfer Dynamics in Molecular Systems, 2nd Revised and Enlarged Edition, Wiley/VCH, Weinheim, 2004.
[13] M.V. Korolkov, J. Manz, Z. Phys. Chem. 217 (2003) 115.
[14] M. Fushitani, M. Bargheer, M. Gühr, N. Schwentner, Phys. Chem. Chem. Phys. 7 (2005) 3143.
[15] M.V. Korolkov, J. Manz, J. Chem. Phys. 120 (2004) 11522.
[16] M.V. Korolkov, J. Manz, Chem. Phys. Lett. 393 (2004) 44.
[17] M. Bargheer, R.B. Gerber, M.V. Korolkov, O. Kühn, J. Manz, M. Schröder, N. Schwentner, Phys. Chem. Chem. Phys. 4 (2002) 5554.
[18] M. Bargheer, M.Y. Niv, R.B. Gerber, N. Schwentner, Phys. Rev. Lett. 89 (2002) 108301.
[19] N.F. Scherer, R.J. Carlson, A. Matro, M. Du, A.J. Ruggiero, V. Romero-Rochin, J.A. Cina, G.R. Fleming, S.A. Rice, J. Chem. Phys. 95 (1992) 1487.
[20] S. Rice, Nature 409 (2001) 422.
[21] R.B. Gerber, P. Jungwirth, Chem. Rev. 99 (1999) 1481.
[22] I.H. Gersonde, H. Gabriel, J. Chem. Phys. 98 (1993) 2094.
[23] V.S. Batista, D.F. Coker, J. Chem. Phys. 106 (1997) 6923.
[24] M. Niv, M. Bargheer, R.B. Gerber, J. Chem. Phys. 113 (2000) 6660.
[25] G. Chaban, R.B. Gerber, M.V. Korolkov, J. Manz, M.Y. Niv, B. Schmidt, J. Phys. Chem. A 105 (2001) 2770.
[26] A.I. Krylov, R.B. Gerber, R.D. Coalson, J. Chem. Phys. 105 (1996) 4626.
[27] D.B. Kokh, A.B. Alekseyev, R.J. Buenker, J. Chem. Phys. 115 (2001) 9298.
[28] D.B. Kokh, A.B. Alekseyev, R.J. Buenker, J. Chem. Phys. 120 (2004) 11549.
[29] L.C. Balling, J.J. Wright, J. Chem. Phys. 79 (1983) 2941.
[30] V. Aquilanti, D. Cappelletti, V. Lorent, E. Luzzatti, F. Pirani, J. Phys. Chem. 97 (1993) 2063.
[31] R.A. Aziz, M.J. Slaman, Mol. Phys. 58 (1986) 679.
[32] M.P. Allen, D.J. Tildesley, Computer Simulation of Liquids, Clarendon Press, Oxford, 1989.
[33] M. Fushitani, N. Schwentner, M. Schröder, O. Kühn, J. Chem. Phys. 124 (2006) 024505.
[34] T. Kiljunen, M. Bargheer, M. Gühr, N. Schwentner, Phys. Chem. Chem. Phys. 6 (2004) 2185.
[35] R. Pausch, M. Heid, T. Chen, H. Schwoerer, W. Kiefer, J. Raman Spectr. 31 (2000) 7.
[36] S. Rutz, R. de Vivie-Riedle, E. Schreiber, Phys. Rev. A 54 (1996) 306.
[37] A.D. Bandrauk, J.-M. Gauthier, J.F. McCann, J. Chem. Phys. 100 (1994) 340.

[38] Z.W. Shen, T. Shen, M. Heid, W. Kiefer, V. Engel, Eur. Phys. J. D 14 (2001) 167.
[39] U. Banin, A. Bartana, S. Ruhman, R. Kosloff, J. Chem. Phys. 101 (1994) 8461.
[40] O. Kühn, D. Malzahn, V. May, Int. J. Quant. Chem. 57 (1996) 343.
[41] K. Bergmann, H. Theuer, B.W. Shore, Rev. Mod. Phys. 70 (1998) 1003.
[42] V.E. Bondybey, C. Fletcher, J. Chem. Phys. 64 (1976) 3615.
[43] M. Bargheer, PhD Thesis, Free University Berlin, 2002. http://www.diss.fu-berlin.de/2002/206/.
[44] J.L. Krause, R.M. Whitnell, K.R. Wilson, Y. Yan, in: J. Manz, L. Wöste (Eds.), Femtosecond Chemistry, vol. 2, Verlag Chemie, Weinheim, 1995, p. 743.
[45] C. Daniel, M.-C. Heitz, J. Manz, C. Ribbing, J. Chem. Phys. 102 (1995) 905.